Journal of the Meteorological Society of Japan

EARLY ONLINE RELEASE

The DOI for this manuscript is
DOI:10.2151/jmsj.2023-004
J-STAGE Advance published date: October 27th, 2022

Effects of dry vegetation coverage estimated from the MODIS Soil Tillage Index on dust occurrence: Verification by surface synoptic observations

Jing WU[1]

Meteorological Research Institute, Tsukuba, Japan
Graduate School of Agricultural and Life Sciences, The University of Tokyo, Tokyo, Japan

Yasunori KUROSAKI

Arid Land Research Center, Tottori University, Tottori, Japan

Tsuyoshi Thomas SEKIYAMA

Meteorological Research Institute, Tsukuba, Japan

and

Takashi MAKI

Meteorological Research Institute, Tsukuba, Japan

July 19, 2022

----

1) Corresponding author: Jing Wu, Meteorological Research Institute, 1-1, Nagemine Tsukuba, Ibaraki 305-0052 JAPAN
Email: wu.jing@mri-jma.go.jp
Tel: +81-29-853-8709
Fax: +81-29-855-2552

Abstract

In drylands, the dry vegetation coverage affects dust occurrence by modulating threshold friction velocity (or wind speed) for dust emission. However, there has been little research into quantifying the effect of dry vegetation coverage on dust occurrence. This study investigated spatial and temporal variations of dust occurrence and three definitions of strong wind frequency over the Gobi Desert and surrounding regions in March and April, months when dust occurrence is frequent, during 2001–2021. We evaluated the effects of variations in dry vegetation on dust occurrence by using the threat scores of forecasted dust occurrences for each strong wind definition. Our results indicate that dry vegetation, which was derived from the MODIS Soil Tillage Index, affects dust occurrence more remarkably in April than in March. In March, land surface parameters such as soil freeze-thaw and snow cover, in addition to dry vegetation coverage, should be considered to explain dust variations in that month. However, use of the threshold wind speed estimated from dry vegetation coverage improved the prediction accuracy of dust occurrence in April. Therefore, we propose that the dry vegetation coverage is a key factor controlling dust occurrence variations in April. The findings imply that estimation of dry vegetation coverage should be applied to dust models.

Keywords dust occurrence; dry vegetation; threshold wind speed; drylands

1. Introduction

Dust occurrence, resulting from wind erosion, has a number of environmental and socioeconomic consequences because of its effects on air pollution, the health of humans and livestock, and the climate (Hagiwara et al, 2020; Hagiwara et al., 2021; Kuribayashi et al., 2019; Middleton, 2017; Miller and Tegen, 1998; Onishi et al., 2012). Many global and regional models have been developed to simulate dust emission, transport, and deposition processes (e.g., Tanaka and Chiba, 2005; Uno et al., 2001; Woodage et al., 2010). However, the performances of different dust emission models also show large uncertainties. For example, Zhao et al. (2022) reported that the global total budget for dust emission among the 18 CMIP6 models has a 5.5-fold range, from 1374 Tg yr^{-1} to 7571 Tg yr^{-1}, depending on the model. As discussed in model intercomparison studies (e.g., Todd et al., 2008; Uno et al., 2006; Wu et al., 2018), we can attribute the diverse results obtained by simulations of dust emission processes to large differences in land surface conditions, in other words, to the lack of confidence in land surface conditions.

Land surface conditions determine erodibility (i.e., susceptibility of soil and land surface to wind erosion), one of the two factors on which dust occurrence depends (UNEP, 1997). Erodibility is influenced by various parameters, including vegetation coverage, snow cover, and soil moisture. The other factor on which dust occurrence depends is erosivity (i.e., ability of wind to cause erosion represented by wind speed), and the relation between erosivity and dust occurrence has been widely studied (e.g., Kurosaki and Mikami, 2003). Although strong winds have been reported to significantly affect dust occurrence in desert regions (Kim and Kai, 2007), many studies have also demonstrated that changes in erodibility, rather than erosivity, control variations in dust occurrence (e.g., Kurosaki et al., 2011; Liu et al., 2020). As one of the erodibility factors for dust occurrence, the presence of vegetation affects the threshold friction velocity, which is defined as the minimum friction velocity required for dust emission to occur. The growth of vegetation in arid and semi-arid regions is largely determined by the summer precipitation, however, the response of vegetation would become weaker due to land degradation (e.g., Sofue et al., 2018). Remote sensing vegetation indices such as the Normalized Difference Vegetation Index (NDVI) have been widely used for monitoring vegetation conditions and analyzing the effect of vegetation on dust occurrence (e.g., Bao et al., 2021; Wu et al., 2016). NDVI is a good indicator of vegetation greenness, however, dry vegetation (i.e., brown vegetation) has significant contributions to the vegetation dynamic (Okin, 2010) and to the dust occurrence (Kurosaki et al., 2011), especially in arid and semi-arid regions. A hypothesis that the presence of dry vegetation in spring, which is the residue of green vegetation from the preceding summer, increases the threshold wind speed and suppresses the probability of dust occurrence was proposed by Kurosaki et al. (2011). The hypothesis was validated by Nandintsetseg and Shinoda (2015) using a process-based ecosystem model. Including the dry vegetation effect in dust simulations can improve dust prediction accuracy, however, the quantitative relation between dry vegetation and the threshold wind speed is not yet well understood because direct detection of dry vegetation cover has been difficult.

Dry vegetation includes both senescent plants (i.e., standing dead plants) and prostrate plants (i.e., litter), which are composed of cellulose, hemicellulose, and lignin. These dry vegetation components have special reflectance characteristics in the short wavelength infrared (SWIR) domain (e.g., Elvidge, 1990). Recently, several vegetation indices derived from SWIR data have been developed to estimate the dry vegetation coverage in arid and semi-arid regions. For example, Kergoat et al. (2015) used the MODIS Soil Tillage Index (STI) to retrieve the dry-season vegetation cover and mass in the Sahel. STI has also been successfully used for the retrieval of the dry vegetation coverage in the desert steppe of Inner Mongolia (Ren et al., 2018; Wang et al., 2019) and in the Gobi Desert of Mongolia (Wu et al., 2021). These studies provide data on continuous spatiotemporal changes of the dry vegetation coverage over wide regions.

In the present study, we investigated interannual variations of dust occurrence and strong winds in the Gobi Desert and surrounding areas in March and April from 2001 to 2021. We defined threshold wind speed in three ways: as a spatiotemporally constant value (6.5 m s^{-1}, often employed in dust models); as a value statistically estimated from surface synoptic observations, which is interannually constant but spatially variable; and as a value estimated by using both synoptic data and the remote sensing index of dry vegetation, which is spatiotemporally variable. We then compared the relationships between dust occurrence and strong wind obtained by using these three different threshold wind speed values with their prediction accuracy, as indicated by their threat scores.

2. Data and Method

2.1 Study region and meteorological data

The region of interest (40°N–47°N, 100°E–120°E) includes the Gobi Desert and grasslands in Mongolia and Inner Mongolia, and adjacent areas, of which land cover types were defined by Kurosaki and Mikami (2005). For meteorological data, we used the 3-hourly present weather and the surface wind speed at a height of 10 m, which are included in surface synoptic observation (SYNOP) reports. Data were extracted from observations at 21 meteorological sites in the study region (Table 1) for the months of March and April during 2001–2021. Dust occurrence is defined by the present weather codes indicating blowing dust (ww = 07, 08) and dust storm (ww = 09, 30–35, 98) (e.g., Kurosaki and Mikami, 2003; Wu et al., 2016), and strong wind is defined as wind speeds exceeding the threshold value for dust occurrence (see section 2.2). We defined the dust occurrence frequency (DOF) as the ratio of the number of observations with dust occurrence to the total number of observations during a given period. Similarly, we defined the strong wind frequency (SWF) as the ratio of the total number of strong wind observations to the total number of observations. Both DOF and SWF are expressed as percentages.

2.2 Threshold wind speed for dust occurrence

The threshold wind speed is the minimum wind speed required for the initiation of sand saltation and dust occurrence. We used three definitions of threshold wind speed in this study. In the first definition, a constant threshold wind speed value of 6.5 m s^{-1} ($u_{6.5}$) is assumed; this value has been widely used in many numerical models (e.g., Dai et al., 2018; Tegen and Fung, 1994; Uno et al., 2001).

In the second definition, the threshold wind speed is statistically estimated from the frequency distribution of the surface wind speed, as proposed by Kurosaki and Mikami (2007) and Kurosaki et al. (2011) (Fig. 1). We determined the wind speed when the dust occurrence probability was 5% ($u_{t5\%}$) by interpolation as the 5th percentile of threshold wind speeds. We employed $u_{t5\%}$ as the threshold wind speed when land surface conditions were close to the most favorable for dust occurrence at a given observatory for the months of March and April during the study period.

In the first definition, threshold wind speed was spatiotemporally constant. In the second definition, it was spatially different but interannually constant from 2001 to 2021, and it differed between March and April. Although in both these definitions, threshold wind speed is interannually constant, it is affected by various land surface conditions, such as soil moisture, surface crust, and vegetation. In the third definition, we accounted for land surface effects by first determining the threshold friction velocity u_{*t} using Eq. (1) (Shao 2008):

$$u_{*t} = u_{*t0}\, f_\lambda(\lambda_v,\ \lambda_s) f_w(\theta) f_{cr}(c_r)\ldots \quad (1)$$

where u_{*t0} is the threshold friction velocity in an idealized situation; λ is the frontal area index, which describes the characteristics of surface roughness elements; θ is the volumetric soil moisture; and c_r describes the surface crustiness. f_λ, f_w and f_{cr} are correction functions for surface-roughness elements, soil moisture, and surface crust, and λ_v and λ_s are the frontal area indices for vegetation and stone, respectively (Darmenova et al., 2009; Foroutan et al., 2017). Although Eq. (1) describes the threshold friction velocity, we cannot obtain friction velocity from synoptic observations. Therefore, we assumed that (1) roughness length z_0 is temporally constant at each observatory and (2) dust emissions always occur under neutral atmospheric conditions. Because wind speed u_z at observation height z is proportional to friction velocity u_*, based on the equation $u_z = u_* \ln(z/z_0)/\kappa$, where κ is von Karman's constant (0.4), the threshold wind speed can be calculated using Eq. (2):

$$
\begin{aligned}
u_t &= u_{t0}\, f_\lambda(\lambda_v, \lambda_s) f_w(\theta) f_{cr}(c_r) \ldots \\
&= u_{t0}\, f_{all}\,. \qquad (2)
\end{aligned}
$$

Here, u_{t0} is the threshold wind speed in the idealized situation, and f_{all} is a correction function comprising all of the correction functions (f_λ, f_w and f_{cr}). Equation (2) can thus be rewritten as described in Eq. (3):

$$u_t = (u_{t0}\, f_{all_{5\%}})\,(f_{all}/f_{all_{5\%}})$$

$$= u_{t5\%}\ (f_{all}/f_{all_{5\%}}). \quad (3)$$

where $f_{all_{5\%}}$ and $u_{t5\%}$ are the 5th percentiles of f_{all} and u_t, respectively. Here, if we assume that the effect of roughness elements on the threshold wind speed is much stronger than that of other factors, so we can neglect the correction functions other than $f_\lambda(\lambda_v,\ \lambda_s)$. Then, the threshold wind speed is expressed as in Eq. (4):

$$u_t = u_{t5\%}\, f_\lambda(\lambda_v,\ \lambda_s)/f_\lambda(\lambda_v,\ \lambda_s)_{5\%}, \quad (4)$$

where $f_\lambda(\lambda_v,\ \lambda_s)_{5\%}$ is the 5th percentile of $f_\lambda(\lambda_v,\ \lambda_s)$. We can expect temporal variation of one of the two roughness elements, stone cover, to be almost none; therefore, its effect can be assumed to be a constant value. Finally, by the third definition, threshold wind speed is estimated from $u_{t5\%}$ and the correction function for vegetation coverage using Eq. (5):

$$u_t = u_{t5\%}\, f_\lambda(\lambda_v\ )/f_\lambda(\lambda_v)_{5\%}. \quad (5)$$

2.3 MODIS-derived dry vegetation coverage and the roughness correction function

The roughness correction function f_λ is calculated as the ratio of the threshold wind friction velocity on a rough land surface to that in the absence of roughness elements (Eq. (6)), as proposed by Raupach et al. (1993):

$$f_\lambda = u_{*t}/u_{*t0} = (1 - m_\gamma \delta_\gamma \lambda)^{1/2}(1 + m_\gamma \beta_\gamma \lambda)^{1/2}, \quad (6)$$

where m_γ is a tuning parameter (<1) to account for the spatial nonuniformity of surface stress, δ_γ is the ratio of the basal to frontal area of the roughness elements, and β_γ controls the stress partition. For sparsely vegetated surfaces, the suggested values of m_γ, δ_γ, and β_γ are 0.16, 1.45, and 202, respectively (Shao, 2008; Wyatt and Nickiing, 1997). The frontal area index λ is calculated from the relation between λ and the vegetation cover fraction (Eq. (7)), as developed by Shao (2008):

$$\lambda = -c_\lambda \ln{(1 - \mathrm{VC_d} \times 0.01)}, \quad (7)$$

where c_λ is an empirical coefficient with a value of ~0.35 (Shao et al., 1996) and $\mathrm{VC_d}$ is the dry vegetation coverage, which is estimated from the MODIS STI as proposed by Wu et al. (2021). We used the MODIS Nadir Bidirectional Reflectance Distribution Function Adjusted Reflectance dataset (MCD43A4, Version 6) with a spatial resolution of 500 m and a daily temporal resolution. STI was calculated as the ratio of band 6 to band 7. We extracted average values for areas of about 10 km × 10 km near each SYNOP observatory, where each observatory was located at the southeast corner of the selected area, to correspond to the meteorological data. We used a maximum value composite procedure to obtain the monthly STI, and converted it to $\mathrm{VC_d}$ using Eq. (8):

$$\mathrm{VC_d} = 54.7\ (\mathrm{STI} - 0.88). \tag{8}$$

Therefore, by the third definition, threshold wind speed (hereinafter, $u_{t(\mathrm{STI})}$) was calculated using Eq. (9):

$$\begin{aligned} u_{t(\mathrm{STI})} &= u_{t5\%}\ f_\lambda(\lambda_v\ )/f_\lambda \\ &= u_{t5\%}\ f_\lambda(\mathrm{STI})/f_\lambda(\mathrm{STI})_{5\%}, \end{aligned} \tag{9}$$

where $f_\lambda(\mathrm{STI})_{5\%}$ is the 5th percentile of $f_\lambda(STI)$, which is obtained from the 5th percentile of STI, for the months of March or April from 2001 to 2021.

2.4 Prediction accuracy

Dust occurrence is predicted when wind speed exceeds the threshold wind speed. To evaluate the dust prediction accuracy, we used the threat score (TS). The TS, which ranges between 0 and 1, is the ratio of the number of correctly predicted events to the total number of events minus the number of correct rejections, as expressed in Eq. (10) (Mikami et al., 2009):

$$\mathrm{TS} \equiv FO/(FO + FX + XO), \tag{10}$$

where FO is the number of predicted dust occurrence events, when wind speeds exceeded the threshold wind speed, that were verified by observations; FX is the number of predicted dust occurrence events that were not observed; and XO is the number of dust occurrence events that were observed but not predicted. We defined TS in three ways ($\mathrm{TS}_{u_{6.5}}$, $\mathrm{TS}_{u_{t5\%}}$, and $\mathrm{TS}_{u_{t(\mathrm{STI})}}$), which were calculated from the number of predicted dust occurrence events obtained by using the three definitions of threshold wind speed.

3. Results and Discussion

3.1 Spatiotemporal variation in dust occurrence and wind conditions

In all regions except grasslands in Inner Mongolia, the DOF was greater in April than in March (Figure 2a–b). High DOF values during 2001–2021 were found in the Gobi Desert in southern Mongolia. The highest DOF value was observed at Tsogt-Ovoo (synoptic observatory 44347, Mongolia), which has previously been observed to be a dust source hotspot (Kurosaki and Mikami, 2007). Relatively high DOFs were also found in grasslands in Inner Mongolia and Mongolia in April. These regions where frequent dust occurrence was observed match those reported in earlier studies (e.g., Wu et al., 2016).

The average DOF over the study region was also higher in April (3.39±1.95%) than in March (2.61±1.51%) (Fig. 2c–d), consistent with previous studies (e.g., Kurosaki & Mikami, 2005; Lee & Kim, 2012), which demonstrated that DOF peaks yearly in April over the Asian dust source regions. The DOFs generally declined from 2001 to 2021 with fluctuations, especially in April. However, in March 2021, the most severe dust events in 10 years were reported (Gui et al., 2021; Yin et al., 2022). In our results, DOF in March increased in 2021, when it was, though not obviously, the third highest value in March in the two decades of the study period (Fig. 2c). However, the DOF reflects only the frequency and not the intensity of dust events.

Temporal changes in the average SWFs calculated using the three definitions for threshold wind speed ($\mathrm{SWF}_{u_{6.5}}$, $\mathrm{SWF}_{u_{t5\%}}$, $\mathrm{SWF}_{u_{t(\mathrm{STI})}}$) showed that strong winds occurred more frequently in April than in March, resulting in higher DOFs in April. Additionally, in either March or April, $\mathrm{SWF}_{u_{6.5}}$ ranged from 10% to about 40%, but $\mathrm{SWF}_{u_{t5\%}}$ and $\mathrm{SWF}_{u_{t(\mathrm{STI})}}$ values were always lower than 20% (Fig. 2c–d). $\mathrm{SWF}_{u_{6.5}}$ was obviously larger than both $\mathrm{SWF}_{u_{t5\%}}$ and $\mathrm{SWF}_{u_{t(\mathrm{STI})}}$; therefore, both $u_{t5\%}$ and $u_{t(\mathrm{STI})}$ were higher than 6.5 m s^{-1}. Consistent with this result, Kurosaki and Mikami (2007) reported that estimated $u_{t5\%}$ from March 1988 to June 2005 was 8.9 m s^{-1} in the Gobi Desert and 9.8 m s^{-1} in northeast Mongolia. According to Liu et al. (2013), threshold wind speeds estimated by selecting the minimum wind speeds when dust events occurred during 1954–2007 in the Inner Mongolian grassland range from 7 to 12.8 m s^{-1}. The comparison with previous studies indicated that the estimated $u_{t5\%}$ and $u_{t(\mathrm{STI})}$ were more accurate than $u_{6.5}$ for preventing dust occurrence

3.2 Effect of dry vegetation coverage on dust occurrence variation

Correlations of DOF with $\mathrm{SWF}_{u_{6.5}}$ ($\mathrm{COR}_{u_{6.5}}$), $\mathrm{SWF}_{u_{t5\%}}$ ($\mathrm{COR}_{u_{t5\%}}$), and $\mathrm{SWF}_{u_{t(\mathrm{STI})}}$ ($\mathrm{COR}_{u_{t(\mathrm{STI})}}$) in April were generally stronger than those in March (Fig. 3). Although the $\mathrm{COR}_{u_{6.5}}$ in both March (R^2 = 0.66) and April (R^2 = 0.82) was significant at the 1% level (p < 0.01), the intercept deviated from the theoretical value of zero. Therefore, we compared only $\mathrm{COR}_{u_{t5\%}}$ and $\mathrm{COR}_{u_{t(\mathrm{STI})}}$. In March, $\mathrm{COR}_{u_{t(\mathrm{STI})}}$ was weaker (R^2 = 0.54) than $\mathrm{COR}_{u_{t5\%}}$ (R^2 = 0.75). This result suggests that the influence of dry vegetation on DOF was not strong in March. This is probably because other factors such as snow cover and soil freeze-thaw process also play important roles in affecting the threshold wind speed for dust occurrence in March (e.g., Kurosaki and Mikami, 2004; Kong et al., 2021). In April, however, $\mathrm{COR}_{u_{t(\mathrm{STI})}}$ (R^2 = 0.88) was stronger than $\mathrm{COR}_{u_{t5\%}}$ (R^2 = 0.78). Moreover, in April, the intercept of $\mathrm{COR}_{u_{t(\mathrm{STI})}}$ approached the theoretical value of zero compared with that of $\mathrm{COR}_{u_{t5\%}}$. The reason for the more theoretical correlation between DOF and $\mathrm{SWF}_{u_{t(\mathrm{STI})}}$ was that effects of the interannual variation of dry vegetation on threshold wind speed were taken into account. The $\mathrm{SWF}_{u_{t(\mathrm{STI})}}$ was more reliable to explain the variation of DOF. This result suggests that the dry vegetation effectively influences DOF in April.

We explored the threat scores at station scale to evaluate the effects of dry vegetation on the interannual variations of DOF. At most stations in March, $\mathrm{TS}_{u_{6.5}}$ values were lower than 0.2 and $\mathrm{TS}_{u_{t5\%}}$ and $\mathrm{TS}_{u_{t(\mathrm{STI})}}$ values were generally higher than 0.2 (Fig. 4a–c). Use of the spatiotemporally constant $u_{6.5}$ resulted in dust occurrence predictions with low accuracy. Threat scores increased from $\mathrm{TS}_{u_{6.5}}$ to $\mathrm{TS}_{u_{t5\%}}$ throughout the study region except at two stations (Tsogt-Ovoo in Mongolia and Ejin-Qi in Inner Mongolia) (Fig. 4d). However, increases from $\mathrm{TS}_{u_{t5\%}}$ to $\mathrm{TS}_{u_{t(\mathrm{STI})}}$ were smaller at 11 observatories, and decreases were found at 10 stations (Fig. 4e). This result indicates that in addition to the dry vegetation coverage, other factors such as snow cover and soil temperature should be considered to explain the variations in dust occurrence. During March, the soil temperature fluctuates above and below 0°C, resulting in frequent cycles of freezing and thawing of soil. The repeated freeze-thaw cycles are disruptive to soil aggregates (e.g., Bullock et al., 1988; Oztas and Fayetorbay, 2003) and thus change the soil structure (e.g., Chamberlain and Gow, 1979). It has been reported that the threshold wind speed became lower during the freeze–thaw periods, thereby enhancing wind erosion and increasing the likelihood of dust occurrence in the Gobi Desert (Abulaiti et al., 2014; Kong et al., 2021). In addition, Kurosaki and Mikami (2004) suggested that snow cover affects the threshold wind speed for dust in East Asia in spring, and its effect is more remarkable in March than in April. Quantifying effects of other land surface parameters on dust occurrence is the subject in need of further study.

In April, $\mathrm{TS}_{u_{6.5}}$ values were generally low, as they were in March, and both $\mathrm{TS}_{u_{t5\%}}$ and

$\mathrm{TS}_{u_{t(\mathrm{STI})}}$ were higher (Fig. 5a–c). $\mathrm{TS}_{u_{t5\%}}$ and $\mathrm{TS}_{u_{t(\mathrm{STI})}}$ values exceeded 0.2 at about 50% and at more than 70% of observatories, respectively. Increases from $\mathrm{TS}_{u_{6.5}}$ to $\mathrm{TS}_{u_{t(\mathrm{STI})}}$ (Fig. 5d) and from $\mathrm{TS}_{u_{t5\%}}$ to $\mathrm{TS}_{u_{t(\mathrm{STI})}}$ (Fig. 5e) occurred at almost all stations. These results suggest that the variation of dry vegetation coverage is the crucial factor in dust occurrence in April through its strong influence on the threshold wind speed. Moreover, increases at stations in the Inner Mongolian grasslands were larger. Since the grasslands are sensitive to climate change and human activities, desertification has been in progress over several years and the degraded grasslands are potentially dust sources (Middleton, 2018; Shinoda et al., 2011). The Chinese government has implemented restoration projects aimed at combating desertification since 2000 (e.g., Li et al., 2017). The environmental policies and projects brought a higher increase of vegetation production in the Inner Mongolian grasslands than the Mongolian grasslands (Zhang et al., 2020). Therefore, dry vegetation coverage showed a more positive effect on dust variations in the Inner Mongolian grasslands. As hypothesized by Kurosaki et al. (2011), the amount of spring dry vegetation remaining from the previous summer is mainly determined by precipitation during the previous year. The amount of spring vegetation is also affected by other factors such as grazing (Kang et al., 2014; Wu et al., 2020). Therefore, the dry vegetation coverage shows both spatial and temporal variability. Because $u_{t(\mathrm{STI})}$ takes account of the variations in dry vegetation coverage, the use of $u_{t(\mathrm{STI})}$ instead of a constant threshold value greatly improves the accuracy of dust occurrence prediction in April.

4. Summary and Conclusion

We examined dust occurrence frequency (DOF) and strong wind frequency (SWF) during 2001–2021 in the Gobi Desert and surrounding regions. We proposed a new method to obtain the threshold wind speed $u_{t(\mathrm{STI})}$ from $u_{t5\%}$ and the MODIS STI-based estimate of dry vegetation coverage. We evaluated the effects of dry vegetation on the threshold wind speed and dust occurrence by threat scores. In March, threat scores based on the estimated $u_{t(\mathrm{STI})}$ were not high over a wide area; thus, other land surface parameters such as snow cover and soil freeze-thaw should be considered to explain the variations in dust occurrence in that month. However, threat scores based on the estimated $u_{t(\mathrm{STI})}$ were high at most stations in April, especially in the Inner Mongolian grasslands, where the average DOFs were about 2%; therefore, the presence of dry vegetation was a key factor determining variations in dust occurrence. Our findings imply that estimation of dry vegetation coverage should be applied to dust models to improve the dust prediction accuracy.

Data Availability Statement

The SYNOP dataset provided by the National Oceanic and Atmospheric Administration are available at https://www.ncei.noaa.gov/data/global-hourly/. The MODIS data can be downloaded in Sentinel Hub EO Browser (https://apps.sentinel-hub.com/eo-browser/).

Acknowledgments

This study was supported by the Arid Land Research Center project titled “Impacts of Climate Change on Drylands: Assessment and Adaptation”, funded by Japan’s Ministry of Education, Culture, Sports, Science, and Technology, the Environment Research and Technology Development Fund (JPMEERF20205001) of the Environmental Restoration and Conservation Agency of Japan, Grants-in-Aid for Scientific Research (Grant Nos. 22K18025 and 22H01310), and the Joint Research Program of the Arid Land Research Center, Tottori University (Grant No. 31C2003).

References

Abulaiti, A., R. Kimura, M. Shinoda, Y. Kurosaki, M. Mikami, M. Ishizuka, Y. Yamada, E. Nishihara, and B. Gantsetseg, 2014: An observational study of saltation and dust emission in a hotspot of Mongolia. *Aeolian Res.*, **15**, 169-176, doi:10.1016/j.aeolia.2014.05.002.

Bao, C., M. Yong, L. Bi, H. Gao, J. Li, Y. Bao, and P. Gomboludev, 2021: Impacts of underlying surface on the dusty weather in Central Inner Mongolian steppe, China. *Earth Space Sci.*, **8**, 9, doi:10.1029/2021EA001672.

Bullock, M. S., S. Nelson, and W. Kemper, 1988: Soil cohesion as affected by freezing, water content, time and tillage. *Soil Sci. Soc. Am. J.*, **52(3)**, 770-776, doi:10.2136/sssaj1988.03615995005200030031x.

Chamberlain, E. J., and A. J. Gow, 1979: Effect of freezing and thawing on the permeability and structure of soils. *Dev. Geotech. Eng.*, **26**, 73-92, doi:10.1016/B978-0-444-41782-4.50012-9.

Dai, T., Y. Cheng, P. Zhang, G. Shi, M. Sekiguchi, K. Suzuki, D. Goto, and T. Nakajima, 2018: Impacts of meteorological nudging on the global dust cycle simulated by NICAM coupled with an aerosol model. *Atmos. Environ.*, **190**, 99-115, doi:10.1016/j.atmosenv.2018.07.016.

Darmenova, K., I. N. Sokolik, Y. Shao, B. Marticorena, and G. Bergametti, 2009: Development of a physically based dust emission module within the Weather Research and Forecasting (WRF) model: Assessment of dust emission parameterizations and input parameters for source regions in Central and East Asia. *J. Geophys. Res.: Atmos.*, **114**, D14, doi:10.1029/2008JD011236.

Elvidge, C. D., 1990: Visible and near infrared reflectance characteristics of dry plant materials. *Int. J. Remote Sen.*, **11(10)**, 1775-1795, doi:10.1080/01431169008955129.

Foroutan, H., J. Young, S. Napelenok, L. Ran, K. Appel, R. Gilliam, and J. Pleim, 2017: Development and evaluation of a physics‐based windblown dust emission scheme implemented in the C MAQ modeling system. *J. Adv. Model. Earth Sy.*, **9(1)**, 585-608, doi:10.1002/2016MS000823.

Gui, K., W. Yao, H. Che, L. An, Y. Zheng, L. Li, H. Zhao, L. Zhang, J. Zhong, Y. Wang, and X. Zhang, 2021: Two mega sand and dust storm events over northern China in March

2021: transport processes, historical ranking and meteorological drivers. *Atmos. Chem. Phys. Discuss.*, **1**, 36, doi:10.5194/acp-2021-933.

Hagiwara, K., T. Matsumoto, P. Tsedendamba, K. Baba, and B. Hoshino, 2020: Distribution of Viable Bacteria in the Dust-Generating Natural Source Area of the Gobi Region, Mongolia. *Atmosphere,* **11(9)**, 893, doi:10.3390/atmos11090893.

Hagiwara, K., T. Matsumoto, P. Tsedendamba, K. Baba, and B. Hoshino, 2021: Bacterial Characteristics of Dust Particle Saltation in Gobi Dust Sites, Mongolia. *Atmosphere,* **12(11)**, 1456, doi:10.3390/atmos12111456.

Kang, J. Y., T. Y. Tanaka, and M. Mikami, 2014: Effect of dead leaves on early spring dust emission in East Asia. *Atmos. Environ.*, **86**, 35-46, doi:10.1016/j.atmosenv.2013.12.007.

Kergoat, L., P. Hiernaux, C. Dardel, C. Pierre, F. Guichard, and A. Kalilou, 2015: Dry-season vegetation mass and cover fraction from SWIR1. 6 and SWIR2. 1 band ratio: Ground-radiometer and MODIS data in the Sahel. *Int. J. Appl. Earth Obs.*, **39**, 56-64, doi:10.1016/j.jag.2015.02.011.

Kim, H. S., and K. Kai, 2007: Recent dust outbreaks in the Taklimakan Desert and their relation to surface wind and land surface condition. *SOLA,* **3**, 69-72, doi:10.2151/sola.2007-018.

Kong, K., B. Nandintsetseg, M. Shinoda, M. Ishizuka, Y. Kurosaki, T. Bat-Oyun, and B. Gantsetseg, 2021: Seasonal variations in threshold wind speed for saltation depending on soil temperature and vegetation: A case study in the Gobi Desert. *Aeolian Res.*, **52**, 100716, doi:10.1016/j.aeolia.2021.100716.

Kurosaki, Y., and M. Mikami, 2003: Recent frequent dust events and their relation to surface wind in East Asia. *Geophys. Res. Lett.*, **30**, 14, doi:10.1029/2003GL017261.

Kurosaki, Y., and M. Mikami, 2004: Effect of snow cover on threshold wind velocity of dust outbreak. *Geophys. Res. Lett.*, **31**, 3, doi:10.1029/2003GL018632.

Kurosaki, Y., and M. Mikami, 2005: Regional difference in the characteristic of dust event in East Asia: Relationship among dust outbreak, surface wind, and land surface condition. *J. Meteorol. Soc. Japan. Ser. II.*, **83**, 1-18, doi.org/10.2151/jmsj.83A.1.

Kurosaki, Y., and M. Mikami, 2007: Threshold wind speed for dust emission in east Asia and its seasonal variations. *J. Geophys. Res.: Atmos.*, **112**, D17, doi:10.1029/2006JD007988.

Kurosaki, Y., M. Shinoda, and M. Mikami, 2011: What caused a recent increase in dust outbreaks over East Asia? *Geophys. Res. Lett.*, **38**, 11, doi:10.1029/2011GL047494.

Kuribayashi, M., K. Kawano, Y. Demura, K. Baba, Y. Sofue, P. Tsedendamba, T. Matsumoto, K. Hagiwara, O. Karthaus, K. Kai, and B. Hoshino, 2019: Imaging of micro-organisms on topsoil particles collected from different landscape in the Gobi Desert. *E3S Web of Conferences*, **99**, 01011, doi:10.1051/e3sconf/20199901011.

Lee, J. J., C. H. Kim, 2012: Roles of surface wind, NDVI and snow cover in the recent changes in Asian dust storm occurrence frequency. *Atmos. Environ.*, **59**, 366-375, doi:10.1016/j.atmosenv.2012.05.022.

Li, S., T. Wang, and C. Yan, 2017: Assessing the role of policies on land-use/cover change from 1965 to 2015 in the Mu Us Sandy Land, northern China. *Sustainability,* **9(7)**, 1164, doi:10.3390/su9071164.

Liu, S., T. Wang, and D. Mouat, 2013: Temporal and spatial characteristics of dust storms in the Xilingol grassland, northern China, during 1954–2007. Reg. Environ. Change, **13(1)**, 43-52, doi:10.1007/s10113-012-0314-5.

Liu, Y., G. Wang, Z. Hu, P. Shi, Y. Lyu, G. Zhang, Y. Gu, Y. Liu, C. Hong, L. Guo, X. Hu, Y. Yang, X. Zhang, H. Zheng, and L. Liu, 2020: Dust storm susceptibility on different land surface types in arid and semiarid regions of northern China. *Atmos. Res.*, **243**, 105031, doi:10.1016/j.atmosres.2020.105031.

Middleton, N. J., 2017: Desert dust hazards: A global review. *Aeolian Res.*, **24**, 53-63, doi:10.1016/j.aeolia.2016.12.001.

Middleton, N., 2018: Rangeland management and climate hazards in drylands: dust storms, desertification and the overgrazing debate. *Nat. hazards,* **92(1)**, 57-70, doi:10.1007/s11069-016-2592-6.

Mikami, M., T. Maki, and T. Y. Tanaka, 2009: Dust forecasting system in JMA. *IOP C. Ser.: Earth Env.*, **7(1)**, 012010, doi:10.1088/1755-1307/7/1/012010.

Miller, R., and I. Tegen, 1998: Climate response to soil dust aerosols. *J. Climate*, **11(12)**, 3247-3267, doi:10.1175/1520-0442(1998)011<3247:CRTSDA>2.0.CO;2.

Nandintsetseg, B., and M. Shinoda, 2015: Land surface memory effects on dust emission in a Mongolian temperate grassland. *J. Geophys. Res.: Biogeo.*, **120(3)**, 414-427, doi:10.1002/2014JG002708.

Okin, G. S., 2010: The contribution of brown vegetation to vegetation dynamics. *Ecology*, **91(3)**, 743-755, doi:10.1890/09-0302.1.

Onishi, K., Y. Kurosaki, S. Otani, A. Yoshida, N. Sugimoto, and Y. Kurozawa, 2012: Atmospheric transport route determines components of Asian dust and health effects in Japan. *Atmos. Environ.*, **49**, 94-102, doi:10.1016/j.atmosenv.2011.12.018.

Oztas, T., and F. Fayetorbay, 2003: Effect of freezing and thawing processes on soil aggregate stability. *Catena*, **52(1)**, 1-8, doi:10.1016/S0341-8162(02)00177-7.

Raupach, M. R., D. A. Gillette, J. F. Leys, 1993: The Effect of Roughness Elements on Wind Erosion Threshold. *J. Geophys. Res.: Atmos.*, **98(D2)**, 3023-3029, doi:10.1029/92JD01922.

Ren, H. R., B. Zhang, X. L. Guo, 2018: Estimation of litter mass in nongrowing seasons in arid grasslands using MODIS satellite data. *Eur. J. Remote Sens.*, **51(1)**, 222-230, doi:10.1080/22797254.2017.1418186.

Shao, Y., 2008: *Physics and modelling of wind erosion. Volume. 37*, Springer Science & Business Media, 472 pp.

Shao, Y., M. R. Raupach, J. F. Leys, 1996: A model for predicting aeolian sand drift and dust entrainment on scales from paddock to region. *Soil Res.*, **34(3)**, 309-342, doi:10.1071/SR9960309.

Shinoda, M., J. Gillies, M. Mikami, and Y. Shao, 2011: Temperate grasslands as a dust source: Knowledge, uncertainties, and challenges. *Aeolian Res.,* **3(3)**, 271-293, doi:10.1016/j.aeolia.2011.07.001.

Sofue, Y., B. Hoshino, Y. Demura, K. Kai, K. Baba, E. Nduati, A. Kondoh, and T. Sternberg, 2018: Satellite monitoring of vegetation response to precipitation and dust storm outbreaks in Gobi Desert regions. *Land***, 7(1)**, 19, doi:10.3390/land7010019.

Tanaka, T. Y., and M. Chiba, 2005: Global simulation of dust aerosol with a chemical transport model, MASINGAR. *J. Meteorol. Soc. Japan. Ser. II.*, **83**, 255-278, doi:10.2151/jmsj.83A.255.

Tegen, I., and I. Fung, 1994: Modeling of mineral dust in the atmosphere: Sources, transport, and optical thickness. *J. Geophys. Res.: Atmos.*, **99(D11)**, 22897-22914, doi:10.1029/94JD01928.

Todd, M. C., D. Bou Karam, C. Cavazos, C. Bouet, B. Heinold, J. M. Baldasano, G. Cautenet, I. Koren, C. Perez, F. Solmon, I. Tegen, P. Tulet, R. Washington, and A. Zakey, 2008: Quantifying uncertainty in estimates of mineral dust flux: An intercomparison of model performance over the Bodélé Depression, northern Chad. *J. Geophys. Res.: Atmos.*, **113**, D24, doi:10.1029/2008JD010476.

United Nations Environment Programme, 1997: *World Atlas of Desertification. 2nd Edition*, Routledge, 192 pp. [Available at https://wedocs.unep.org/20.500.11822/30300.]

Uno, I., H. Amano, S. Emori, K. Kinoshita, I. Matsui, N. Sugimoto, 2001: Trans-Pacific yellow sand transport observed in April 1998: A numerical simulation. *J. Geophys. Res.: Atmos.*, **106(D16)**, 18331-18344. doi:10.1029/2000JD900748.

Uno, I., Z. Wang, M. Chiba, Y. Chun, S. L. Gong, Y. Hara, E. Jung, S. S. Lee, M. Liu, M. Mikami, S. Music, S. Nickovic, S. Satake, Y. Shao, Z. Song, N. Sugimoto, T. Y. Tanaka, and D. L. Westphal, 2006: Dust model intercomparison (DMIP) study over Asia: Overview. *J. Geophys. Res.: Atmos.*, **111**, D12. doi:10.1029/2005JD006575.

Wang, G. Z., J. P. Wang, X. Y. Zou, G. Q. Chai, M. Q. Wu, and Z. L. Wang, 2019: Estimating the fractional cover of photosynthetic vegetation, non-photosynthetic vegetation and bare soil from MODIS data: Assessing the applicability of the NDVI-DFI model in the typical Xilingol grasslands. *Int. J. Appl. Earth Obs.*, **76**, 154-166. doi:10.1016/j.jag.2018.11.006.

Woodage, M., A. Slingo, S. Woodward, and R. Comer, 2010: UK HiGEM: simulations of desert dust and biomass burning aerosols with a high-resolution atmospheric GCM. *J. Climate*, **23(7)**, 1636-1659. doi:10.1175/2009JCLI2994.1.

Wu, C., Z. Lin, X. Liu, Y. Li, Z. Lu, and M. Wu, 2018: Can climate models reproduce the decadal change of dust aerosol in East Asia? *Geophys. Res. Lett.*, **45(18)**, 9953-9962. doi:10.1029/2018GL079376.

Wu, J., Y. Kurosaki, M. Shinoda, and K. Kai, 2016: Regional characteristics of recent dust occurrence and its controlling factors in East Asia. *SOLA,* **12**, 187-191.

doi:10.2151/sola.2016-038.

Wu, J., Y. Kurosaki, and C. Du, 2020: Evaluation of climatic and anthropogenic impacts on dust erodibility: A case study in Xilingol Grassland, China. *Sustainability*, **12(2)**, 629. doi:10.3390/su12020629.

Wu, J., Y. Kurosaki, B. Gantsetseg, M. Ishizuka, T. T. Sekiyama, B. Buyantogtokh, and J. Liu, 2021: Estimation of dry vegetation cover and mass from MODIS data: Verification by roughness length and sand saltation threshold. *Int. J. Appl. Earth Obs.*, **102**, 102417. doi:10.1016/j.jag.2021.102417.

Wyatt, V., and W. Nickiing, 1997: Drag and shear stress partitioning in sparse desert creosote communities. *Can. J. Earth Sci.*, **34(11)**, 1486-1498. doi:10.1139/e17-121.

Yin, Z., Y. Wan, Y. Zhang, and H. Wang, 2022: Why super sandstorm 2021 in North China? *Natl. Sci. Rev.*, **9(3)**, nwab165. doi:10.1093/nsr/nwab165.

Zhao, A., C. L. Ryder, and L. J. Wilcox, 2022: How well do the CMIP6 models simulate dust aerosols? *Atmos. Chem. Phys.*, **22(3)**, 2095-2119. doi:10.5194/acp-22-2095-2022.

Zhang, Y., Q. Wang, Z. Wang, Y. Yang, and J. Li, 2020: Impact of human activities and climate change on the grassland dynamics under different regime policies in the Mongolian Plateau. *Sci. Total Environ.,* **698**, 134304, doi:10.1016/j.scitotenv.2019.134304.

List of Figures

three circle sizes indicate threat scores of 0–0.2 (blue), 0.2–0.4 (yellow), and >0.4 (red). Increases and decreases between (d) $\mathrm{TS}_{u_{6.5}}$ and $\mathrm{TS}_{u_{t5\%}}$, and (e) $\mathrm{TS}_{u_{t5\%}}$ and $\mathrm{TS}_{u_{t(\mathrm{STI})}}$ are shown by triangles and inverted triangles, respectively, and the color indicates the magnitude of the change.

Fig. 5 Same as Figure 4 but for April.

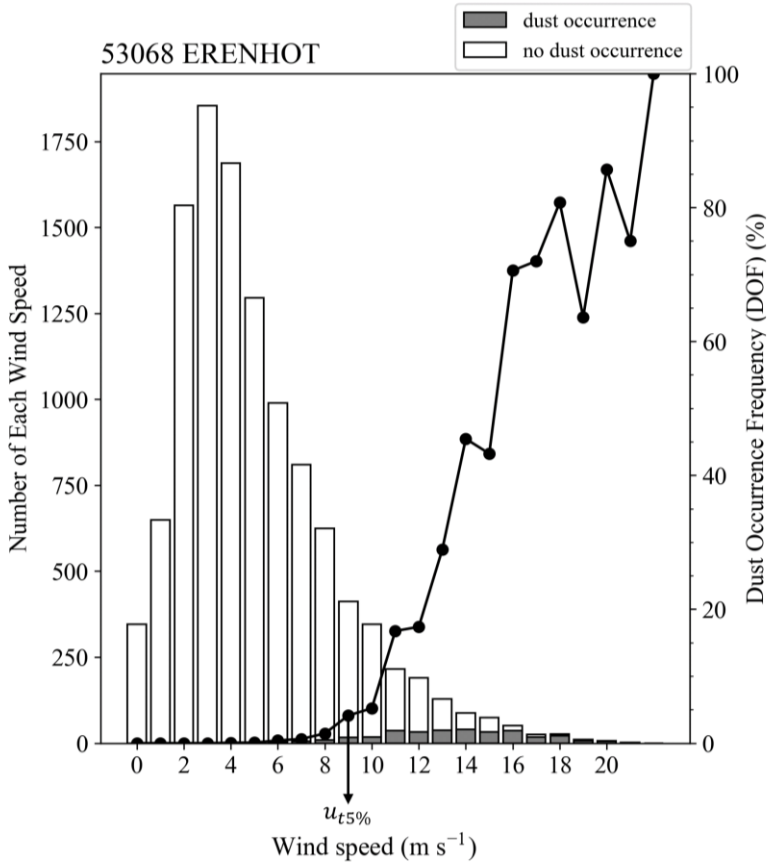

Fig. 1 Frequency distribution of observed wind speeds at a synoptic weather observatory (53068 Erenhot, 43.65°N, 112°E) in April during 2001–2021. Filled and open bars indicate frequencies with and without dust occurrence, respectively. The solid dots on the line indicate the dust occurrence frequency at each wind speed.

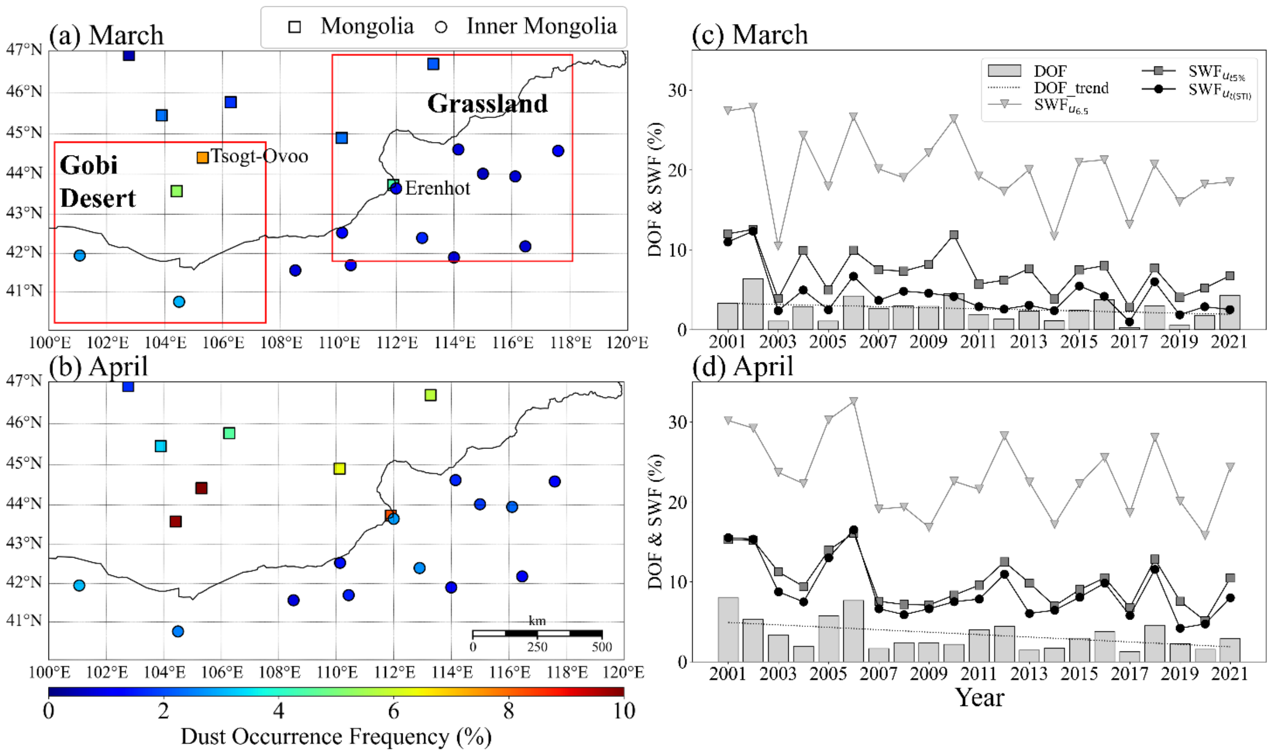

Fig. 2 Spatial distribution of the average dust occurrence frequency at SYNOP observatories in Mongolia (squares) and Inner Mongolia (circles) in (a) March and (b) April during 2001–2021. The line shows the border between Mongolia (to the north) and Inner Mongolia, and the red boxes in (a) indicate the Gobi Desert and grasslands areas. Temporal variations of the average dust occurrence frequency (DOF. gray bars; trend, dotted line) and strong wind frequencies ($SWF_{u_{6.5}}$, triangles; $SWF_{u_{t5\%}}$, squares; and $SWF_{u_{t(\mathrm{STI})}}$, circles) over the study region in (c) March and (d) April during 2001–2021.

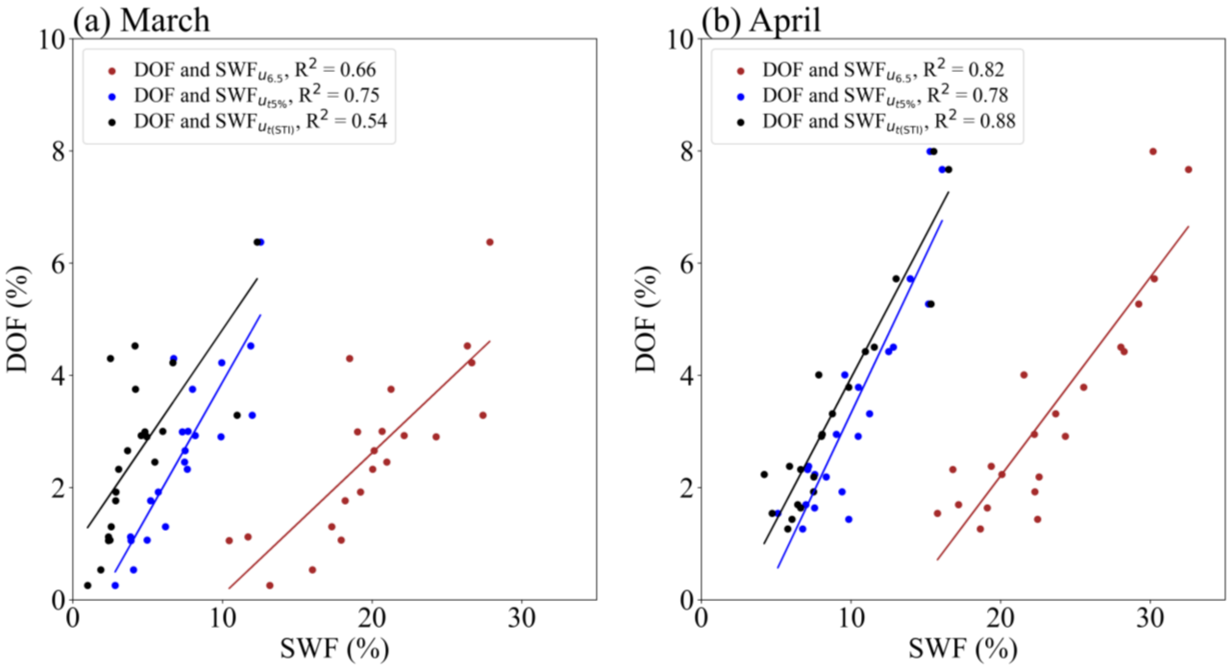

Fig. 3 Scatter diagrams of DOF and $\mathrm{SWF}_{u_{6.5}}$ (brown), $\mathrm{SWF}_{u_{t5\%}}$ (blue), and $\mathrm{SWF}_{u_{t(\mathrm{STI})}}$ (black) in (a) March and (b) April during 2001–2021.

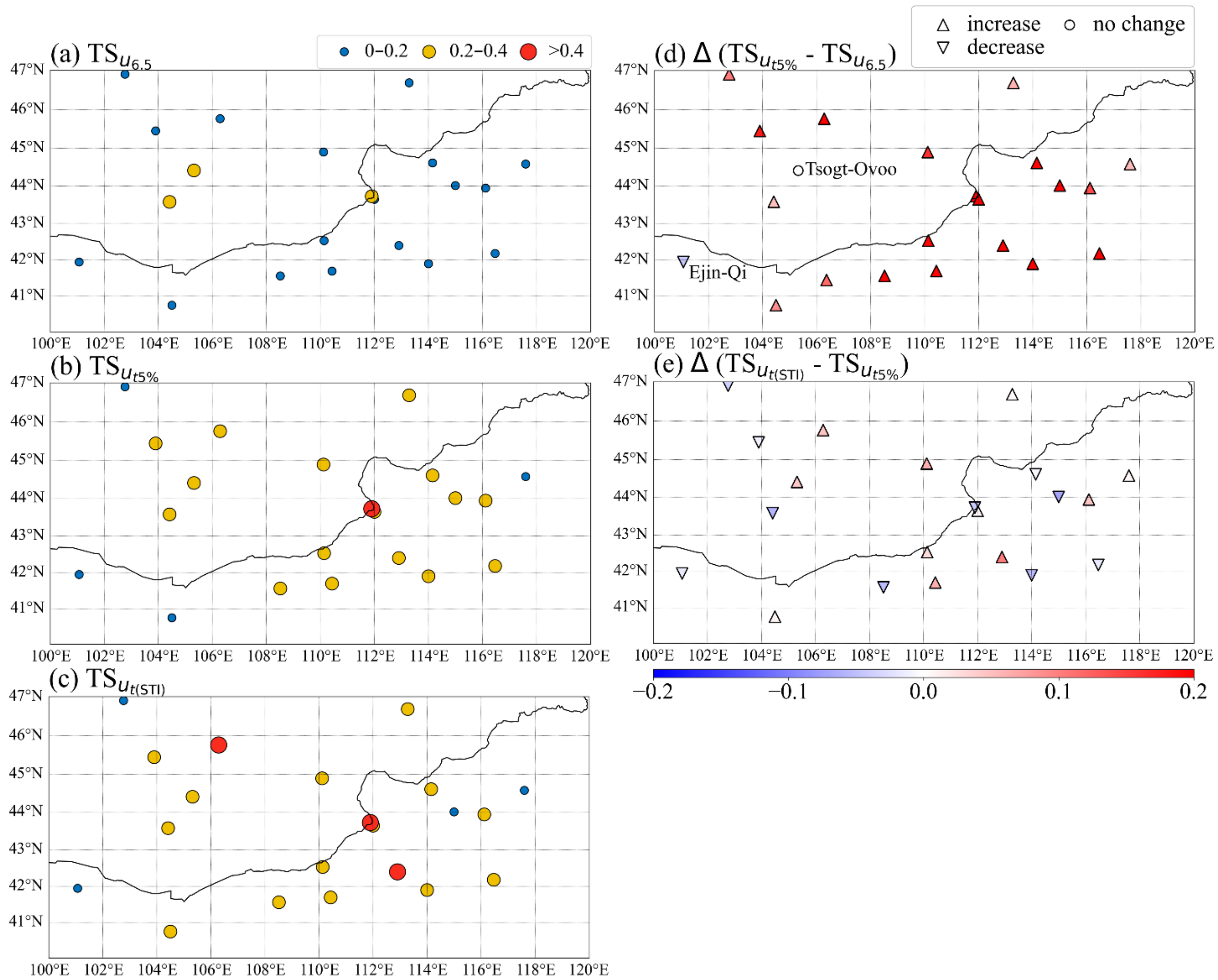

Fig. 4 Spatial distributions of threat scores for dust occurrence at the SYNOP observatories in our study area in March: (a) $TS_{u_{6.5}}$, (b) $TS_{u_{t5\%}}$, and (c) $TS_{u_{t(STI)}}$. The three circle sizes indicate threat scores of 0–0.2 (blue), 0.2–0.4 (yellow), and >0.4 (red). Increases and decreases between (d) $TS_{u_{6.5}}$ and $TS_{u_{t5\%}}$, and (e) $TS_{u_{t5\%}}$ and $TS_{u_{t(STI)}}$ are shown by triangles and inverted triangles, respectively, and the color indicates the magnitude of the change.

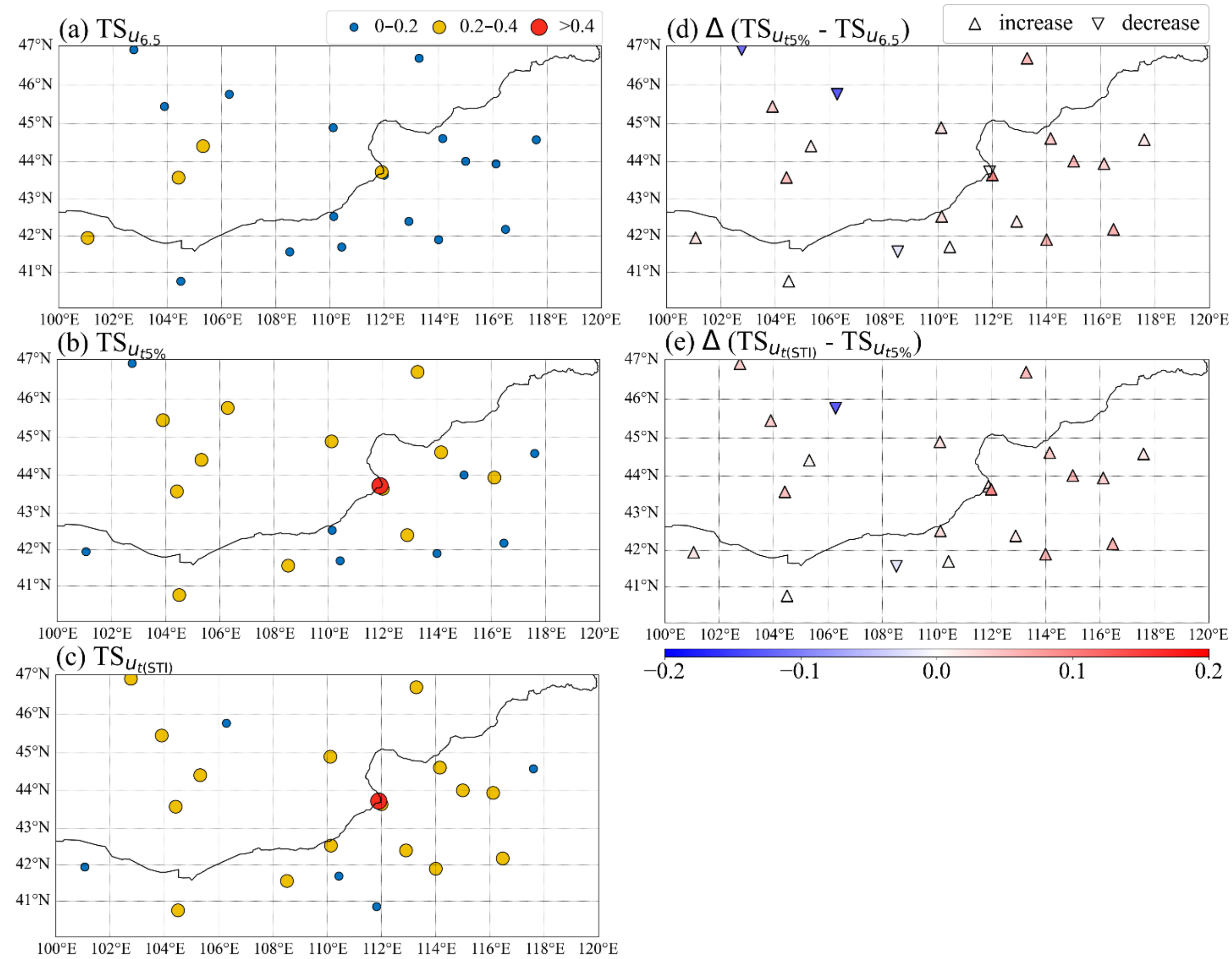

Fig. 5 Same as Figure 4 but for April.

List of Tables

Table 1 Names and locations of the SYNOP meteorological stations used in this study.

Mongolia			Inner Mongolia, China		
Name	Longitude	Latitude	Name	Longitude	Latitude
Hujirt	102.77	46.90	Ejin Qi	101.07	41.95
Baruun-urt	113.28	46.68	Bayan Mod	104.50	40.75
Saikhan-Ovoo	103.90	45.45	Erenhot	112.00	43.65
Mandalgovi	106.28	45.77	Naran Bulag	114.15	44.62
Tsogt-Ovoo	105.32	44.42	Mandal	110.13	42.53
Sainshand	110.12	44.90	Abag Qi	115.00	44.02
Zamyn-Uud	111.90	43.73	Jurh	112.90	42.40
Dalanzadgad	104.42	43.58	Haliut	108.52	45.57
			Bailing-Miao	110.43	41.70
			Huade	114.00	41.90
			Xi Ujimqin Qi	117.60	44.58
			Xilin Hot	116.12	43.95
			Duolun	116.47	42.18